Simulating propagation of separated wave modes in general anisotropic media, Part II: qS-wave propagators[a]

[a]Published in Geophysics, 81, no. 2, C39-C52, (2016)

Jiubing Cheng[1] *and Wei Kang*[2]

ABSTRACT

Shear waves, especially converted modes in multicomponent seismic data, provide significant information that allows better delineation of geological structures and characterization of petroleum reservoirs. Seismic imaging and inversion based upon the elastic wave equation involve high computational cost and many challenges in decoupling the wave modes and estimating so many model parameters. For transversely isotropic media, shear waves can be designated as pure SH and quasi-SV modes. Through two different similarity transformations to the Christoffel equation aiming to project the vector displacement wavefields onto the isotropic references of the polarization directions, we derive simplified second-order systems (i.e., pseudo-pure-mode wave equations) for SH- and qSV-waves, respectively. The first system propagates a vector wavefield with two horizontal components, of which the summation produces pure-mode scalar SH-wave data, while the second propagates a vector wavefield with a summed horizontal component and a vertical component, of which the final summation produces a scalar field dominated by qSV-waves in energy. The simulated SH- or qSV-wave has the same kinematics as its counterpart in the elastic wavefield. As explained in our previous paper (part I), we can obtain completely separated scalar qSV-wave fields after spatial filtering the pseudo-pure-mode qSV-wave fields. Synthetic examples demonstrate that these wave propagators provide efficient and flexible tools for qS-wave extrapolation in general transversely isotropic media.

INTRODUCTION

Ultrasonic laboratory studies as well as seismic field investigations have shown that many geological materials and subsurface structures are elastically anisotropic. It is well known that a shear wave passing through an anisotropic material splits into two mutually orthogonal waves, which propagate at different velocities. Therefore, seismic waves propagate through the earth as a superposition of three body wave modes, one P-wave and two S-waves. Generally they are polarized neither parallel to nor perpendicular to the direction of wave travel, thus are called quasi-P (qP) and

quasi-S (qS) waves, with quasi- means similar to but not exactly. P- and S-waves were originally named for their arrival times, with P for the first (primary) and S for the second. Today, the indicators P and S are often connected with polarization, i.e., P with compressional (or longitudinal) and S with shear (or transverse), with the specification SH and SV for waves with transverse displacements in the horizontal and vertical planes, respectively (Winterstein, 1990). For vertical transversely isotropic (VTI) media, one often uses this terminology with qP, qSV, and SH, since the first two of these waves are generally not purely longitudinal and transverse, respectively.

Because seismic anisotropy by nature is an elastic phenomenon, the full elastic wave equation is usually more accurate for wavefield extrapolation than the acoustic equation. However, seismic imaging using the elastic wave equation involve high computational cost and many challenges in decoupling wave modes to get physically interpretable images of the subsurface (Dellinger and Etgen, 1990; Zhang and McMechan, 2010; Yan and Sava, 2011; Cheng and Fomel, 2014). For real-sized applications of seismic imaging and inversion, it is necessary to resort to a simplified description of wave propagation in anisotropic media.

Pseudoacoustic wave equations are the most common approximations made to mono-component (mainly pressure) seismic data. They are derived by setting the qS-wave phase velocity along the symmetry axis to zero for VTI or orthorhombic media (Alkhalifah, 2000, 2003; Duveneck and Bakker, 2011). Pseudoacoustic wave equations describe the kinematic signatures of qP-waves with sufficient accuracy and are simpler than their elastic counterparts, which leads to computational savings in practice (Zhou et al., 2006; Fletcher et al., 2009; Zhang and Zhang, 2011). They also have fewer parameters, which is important for inversion. However, we note several limitations of the acoustic anisotropic wave equation. First, acoustic approximation does not prevent the propagation of qS-waves in directions other than the symmetry axis (Grechka et al., 2004; Zhang et al., 2005); the residual qS-waves are regarded as artifacts in the framework of acoustic modeling, reverse-time migration (RTM) and full waveform inversion (FWI) (Alkhalifah, 2000; Zhang et al., 2009; Operto et al., 2009). Second, stability analysis based on requiring the stiffness tensor to remain positive definite (Helbig, 1994) shows that wavefield extrapolation in a pseudo-acoustic TI or orthorhombic medium can become unstable (Alkhalifah, 2000; Grechka et al., 2004; Fowler and King, 2011). Alternatively, qP- and qS-wave propagation can be formally decoupled in the wavenumber domain to yield pure-mode pseudodifferential equations (Liu et al., 2009; Du et al., 2014). Unfortunately, these equations in time-space domain cannot be solved with traditional numerical schemes. Through factorizing and approximating the qP-qSV dispersion relations or phase velocities, many authors proposed to simulate propagation of scalar pure-mode waves using mixed-domain recursive integral operators (Etgen and Brandsberg-Dahl, 2009; Liu et al., 2009; Zhang and Zhang, 2009; Crawley et al., 2010; Fowler et al., 2010; Chu et al., 2011; Pestana et al., 2011; Zhan et al., 2012; Fomel et al., 2013) or novel finite-difference operators (Song et al., 2013). To avoid solving the pseudodifferential equation, Xu and Zhou (2014) proposed a nonlinear wave equation for a pseudo-acoustic qP-wave with an auxiliary scalar operator depending on the material parameters and the phase

direction of the propagation at each spatial location.

Multicomponent seismic data are increasingly acquired on land and at the ocean bottom to better delineate geological structures and to characterize oil and gas reservoirs (Li, 1997; Thomsen, 1999; Cary, 2001; Stewart et al., 2002; Hardage et al., 2011). The development of unconventional reservoirs and the microseismic monitoring of hydraulic fracturing has led to more interest in shear waves because microseismic sources emit strong shear energy that is routinely recorded by three-component geophones (Maxwell, 2010) and is widely recognized as being useful for locating microseismic events and estimating their focal mechanisms (Baig and Urbancic, 2010; Grechka and Yaskevich, 2014). In fact, anisotropic phenomena are especially noticeable in shear and mode-converted wavefields. Therefore, modeling of anisotropic shear waves may be important both theoretically and practically. As we know, the pseudoacoustic approximation is not appropriate for qS-waves. In addition to amplitude errors, the kinematic accuracy of qS-waves is reduced if we use the existing numerical schemes based on factorizing and approximating the dispersion relations or phase velocities.

In kinematics, there are various forms equivalent to the original elastic wave equations. In our previous paper (part I), we derived the pseudo-pure-mode wave equation for qP-waves by applying a particular similarity transformation to the Christoffel equation and demonstrated its features in describing wave propagation for TI and orthorhombic media. Except for its application to scalar qP-wave RTM (Cheng and Kang, 2014), the pseudo-pure-mode wave equation provides new insight into developing approaches for multicomponent qP-wave inversion (Djebbi and Alkhalifah, 2014). The same theoretical framework described in part I is applied to qS-waves in this paper. First we derive the pseudo-pure-mode wave equations for qS-waves in TI media through new similarity transformations to the original Christoffel equation. Numerical examples demonstrate the features of the proposed qS-wave propagators in 2D and 3D TI media. Then we discuss the dynamic features of the pseudo-pure-mode qS-wave equations and the challenges to extending them to anisotropic media with lower symmetry.

PHASE VELOCITY AND POLARIZATION CHARACTERISTICS

Following Carcione (2007), we denote the spatial variables x, y and z of a Cartesian system by the indices $i, j, \ldots = 1$, 2 and 3, respectively, the position vector by $\mathbf{x}$, a partial derivative with respect to a variable x_i with ∂_i, and the first and second time derivatives with ∂_t and ∂_{tt}. Matrix transposition is denoted by the superscript "$\top$". We also denote the scalar and matrix products by the symbol "$\cdot$", and the gradient operator by $\bigtriangledown$.

The wave equation in a general heterogeneous anisotropic medium can be expressed as

$$\rho\partial_{tt}\mathbf{u} = [\bigtriangledown\mathbf{C}\bigtriangledown^{\top}]\mathbf{u} + \mathbf{f}, \tag{1}$$

where $\mathbf{u} = (u_x, u_y, u_z)^\top$ is the particle displacement vector, $\mathbf{f} = (f_x, f_y, f_z)^\top$ represents the force term, ρ the density, $\mathbf{C}$ the matrix representing the stiffness tensor in a two-index notation called the Voigt recipe. The gradient operator has the following matrix representation:

$$\bigtriangledown = \begin{pmatrix} \partial_x & 0 & 0 & 0 & \partial_z & \partial_y \\ 0 & \partial_y & 0 & \partial_z & 0 & \partial_x \\ 0 & 0 & \partial_z & \partial_y & \partial_x & 0 \end{pmatrix}. \tag{2}$$

Neglecting the source term, a plane-wave analysis of the elastic wave equation yields the Christoffel equation,

$$\widetilde{\mathbf{\Gamma}}\widetilde{\mathbf{u}} = \rho\omega^2\widetilde{\mathbf{u}}, \tag{3}$$

where ω is the angular frequency and $\widetilde{\mathbf{u}} = (\widetilde{u}_x, \widetilde{u}_y, \widetilde{u}_z)^\top$ is the wavefield in Fourier domain; the wavenumber-domain counterpart of the gradient operator is written as

$$\widetilde{\mathbf{L}} = \begin{pmatrix} k_x & 0 & 0 & 0 & k_z & k_y \\ 0 & k_y & 0 & k_z & 0 & k_x \\ 0 & 0 & k_z & k_y & k_x & 0 \end{pmatrix}, \tag{4}$$

in which the propagation direction is specified by the wave vector $\mathbf{k} = (k_x, k_y, k_z)^\top$, and the symmetric Christoffel matrix $\widetilde{\Gamma} = \widetilde{\mathbf{L}}\mathbf{C}\widetilde{\mathbf{L}}^\top$ satisfies:

$$\widetilde{\Gamma} = \begin{pmatrix} C_{11}{k_x}^2 + C_{66}{k_y}^2 + C_{55}{k_z}^2 & (C_{12}+C_{66})k_xk_y & (C_{13}+C_{55})k_xk_z \\ (C_{12}+C_{66})k_xk_y & C_{66}{k_x}^2 + C_{22}{k_y}^2 + C_{44}{k_z}^2 & (C_{23}+C_{44})k_yk_z \\ (C_{13}+C_{55})k_xk_z & (C_{23}+C_{44})k_yk_z & C_{55}{k_x}^2 + C_{44}{k_y}^2 + C_{33}{k_z}^2 \end{pmatrix}. \tag{5}$$

The squared phase (or normal) velocities ${V^2}_q (q = 1, 2, 3)$ are eigenvalues of the Christoffel matrix. The inequalitities

$$V_1(\mathbf{k}) \geq V_2(\mathbf{k}) \geq V_2(\mathbf{k}) \tag{6}$$

establish the types of waves. Except for anomalous cases of elastic anisotropy, which are of little interest in geophysics, the qP-wave ($q = 1$) usually is faster than qS-waves ($q = 2, 3$) and the equation

$$V_1(\mathbf{k}) = V_2(\mathbf{k}) \tag{7}$$

is a great rarity (Yu et al., 1993). However, the equation

$$V_2(\mathbf{k}) = V_3(\mathbf{k}) \tag{8}$$

is a common event because the phase velocity surfaces (corresponding to qS1 and qS2 waves) can touch or intersect each other (Musgrave, 1970). Directions of wave normals along which the two phase velocities are equal to each other are called acoustic axes or singularity directions. For the shear singularities, the Christoffel matrix is degenerate. Crampin (1991) distinguished three kinds of singularity: point, kiss and line. In point and kiss singularities, the phase velocity surfaces touch at a single point, while in line singularities they intersect. Generally, inserting a nondegenerate eigenvalue back into the Christoffel equation gives ratios of the components of $\mathbf{u}$, which specify polarization

along a given phase direction for a given wave mode. The polarization consists of the geometrical properties of the particle motion, including trajectory shape and spatial orientation, but excludes magnitudes of the motion. Polarization of an isolated body wave in a noise-free perfectly elastic medium is linear (Winterstein, 1990). In isotropic media, polarizations of such body waves are either parallel to the direction of wave travel, for P-waves, or perpendicular to it, for S-waves. The polarization vectors of the S-wave may take an arbitrary orientation in the plane orthogonal to the P-wave polarization vector. In anisotropic media, however, the polarizations are often neither parallel nor perpendicular to the direction of wave propagation. Whether the medium is anisotropic or not, the polarizations of the three wave modes are always mutually orthogonal for a given propagation direction. So we may separate the elastic wavefield into single-mode scalar fields using the polarization-based projection:

$$\widetilde{w} = i\mathbf{a}_w \cdot \widetilde{\mathbf{u}}, \tag{9}$$

with $\mathbf{a}_w$ representing the normalized polarization vector of the given mode $w = \{qP, qS_1, qS_2\}$ (Dellinger, 1991).

In practice, horizontally polarized (or SH) and vertically polarized (or SV) are likely to be the most useful S-wave modes when consideration is restricted to isotropic or TI media, in which all rays lie in symmetry planes. For isotropic media, the above polarization-based projection is material-independent, because the following vectors related to the wave vector $\mathbf{k}$, i.e.,

$$\mathbf{e}_1 = (k_x, k_y, k_z)^\top, \qquad \mathbf{e}_2 = (-k_y, k_x, 0)^\top \qquad \text{and} \qquad \mathbf{e}_3 = (k_x k_z, k_y k_z, -(k_x^2 + k_y^2))^\top, \tag{10}$$

indicate the polarization direction of pure P-, SH- and SV-wave, respectively. On the contrary, for anisotropic media, the polarization-based projection depends on local material parameters, because the polarizations are generally specified by the eigenvectors of the original Christoffel equation. For a VTI medium, the stiffness coefficients satisfy: $C_{12} = C_{11} - 2C_{66}$, $C_{22} = C_{11}$, $C_{23} = C_{13}$ and $C_{55} = C_{44}$. In this case, people still prefer to designate the qS-waves as SH-like and SV-like modes due to the following fact: The use of qS1 and qS2 distinguished by phase velocities does not always give continuous polarization surfaces, while the use of SV and SH distinguished by polarization does, except at the kiss singularity at $k_x = k_y = 0$ (Crampin and Yedlin, 1981; Zhang and McMechan, 2010). In this case, the SH-waves polarize perpendicular to the symmetry plane and are pure, and the SV-waves polarize in symmetry planes and are usually quasi-shear. As shown in Figure 1, for both qP and qSV modes, the polarization directions in a VTI material deviate from those in the corresponding isotropic (reference) medium in most propagation directions, but no deviation exists for the SH mode in any direction for either medium. To our interest, the polarization deviations of qP- or qSV-waves between an ordinary VTI medium and its isotropic reference are usually very small, although exceptions are possible (Thomsen, 1986; Tsvankin and Chesnokov, 1990). In addition, taking vectors $\mathbf{e}_1$, $\mathbf{e}_2$ and $\mathbf{e}_3$ as the three mutually perpendicular polarization vectors in the unperturbed isotropic medium, approximate formulas for the qP- and qS-wave polarizations in an

arbitrary anisotropic medium can be developed using perturbation theory (Cerveny and Jech, 1982; Psencik and Gajewski, 1998; Farra, 2001).

To provide for more possibilities and flexibility in describing single-mode wave propagation in anisotropic media, Cheng and Kang (2014) suggest splitting the one-step polarization-based projection into two steps, of which the first step implicitly implements partial wave-mode separation during wavefield extrapolation with a transformed wave equation, while the second step is designed to correct the projection deviation due to the approximation of polarization directions. The transformed wave equation (that they called a pseudo-pure-mode qP-wave equation) was derived from the original Christoffel equation through a similarity transformation aiming to project the displacement wavefield onto the isotropic (reference) polarization direction indicated by $\mathbf{e}_1$. In this paper, taking another two orthogonal vectors in equation 10, namely $\mathbf{e}_2$ and $\mathbf{e}_3$, as the reference polarization directions for SH- and qSV-waves, we apply the same strategy to derive simplified wave equations for these qS-wave modes in general TI media.

PURE-MODE SH-WAVE EQUATION

Pure SH-waves horizontally polarize in the planes perpendicular to the symmetry axis of VTI media with $u_z \equiv 0$, so we introduce a similarity transformation to the Christoffel matrix ignoring the vertical component, i.e.,

$$\widetilde{\widetilde{\mathbf{\Gamma}}}_{\mathbf{m}} = \mathbf{M}\widetilde{\mathbf{\Gamma}}_2\mathbf{M}^{-1}, \tag{11}$$

with a generally invertible 2×2 matrix $\mathbf{M}$ related to the reference polarization direction $\mathbf{e}_2$:

$$\mathbf{M} = \begin{pmatrix} -k_y & 0 \\ 0 & k_x \end{pmatrix}, \tag{12}$$

and

$$\widetilde{\Gamma}_2 = \begin{pmatrix} C_{11}{k_x}^2 + C_{66}{k_y}^2 + C_{44}{k_z}^2 & (C_{12}+C_{66})k_xk_y \\ (C_{12}+C_{66})k_xk_y & C_{66}{k_x}^2 + C_{22}{k_y}^2 + C_{44}{k_z}^2 \end{pmatrix}. \tag{13}$$

Accordingly, we derive a transformed Christoffel equation,

$$\widetilde{\widetilde{\mathbf{\Gamma}}}_{\mathbf{m}}\widetilde{\widetilde{\mathbf{u}}} = \rho\omega^2\widetilde{\widetilde{\mathbf{u}}}, \tag{14}$$

for the SH-wave mode:

$$\widetilde{\widetilde{\mathbf{u}}} = \mathbf{M}\widetilde{\mathbf{u}}_2, \tag{15}$$

in which $\widetilde{\mathbf{u}}_2 = (\widetilde{u}_x, \widetilde{u}_y)^\top$ represents the horizontal components of the original elastic wavefields, and $\widetilde{\widetilde{\mathbf{u}}} = (\widetilde{\widetilde{u}}_x, \widetilde{\widetilde{u}}_y)^\top$ represents the horizontal components of the transformed wavefields. Note that the matrix $\mathbf{M}$ will be not invertible when $k_x = 0$ or/and $k_y = 0$. These special directions don't affect the derivation of the pseudo-pure-mode wave equation for the following reasons: First, we don't directly project the elastic wavefield into the wavenumber-domain, but instead apply the similarity transformation to the

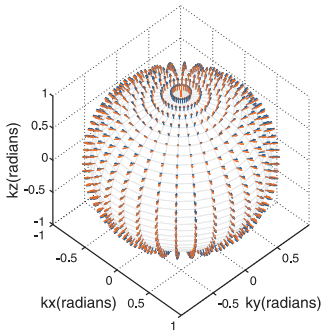

(a)

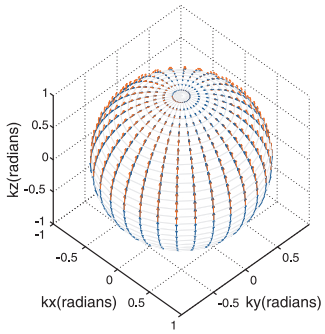

(b)

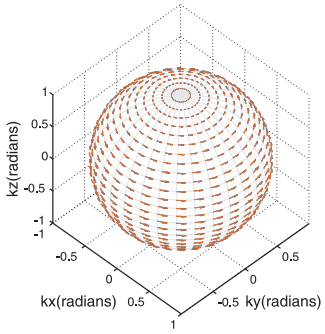

(c)

Figure 1: Polarization vectors in a 3D VTI material with $v_{p0} = 3.0$ km/s, $v_{s0} = 1.5$ km/s, $\epsilon = 0.25$, and $\delta = -0.29$. Its isotropic reference medium is determined by setting $\epsilon = 0$ and $\delta = 0$. One can observe polarization deviations between VTI (red) and its isotropic reference (blue) media for (a) P- and (b) S-waves in most propagation directions, but no deviation for (c) SH-waves in any direction.

Christoffel equation and eventually inverse the transformed Christoffell equation back into the time-space-domain. Second, the original Christofell matrix $\widetilde{\Gamma}_2$ automatically becomes a diagonal matrix in these directions, so the similarity transformation is not actually needed for the corresponding wavenumber components.

Note the similarity transformation does not change the eigenvalue of the Christoffel matrix corresponding to the SH-wave and, thus, introduces no kinematic error for this wave mode. We also can obtain a kinematically equivalent Christoffel equation if $\mathbf{M}$ is constructed using the normalized form of $\mathbf{e}_2$ to ensure all spatial frequencies are uniformly scaled. For a locally smooth medium, applying an inverse Fourier transform to equation 14, we obtain a linear second-order system in the time-space domain:

$$\rho\partial_{tt}\overline{\mathbf{u}} = \overline{\mathbf{\Gamma}}_{\mathbf{m}}\overline{\mathbf{u}}, \tag{16}$$

or in its extended form:

$$\begin{aligned}\rho\partial_{tt}\overline{u}_x &= C_{11}\partial_{xx}\overline{u}_x + C_{66}\partial_{yy}\overline{u}_x + C_{44}\partial_{zz}\overline{u}_x - (C_{11}-C_{66})\partial_{yy}\overline{u}_y,\\ \rho\partial_{tt}\overline{u}_y &= C_{66}\partial_{xx}\overline{u}_y + C_{11}\partial_{yy}\overline{u}_y + C_{44}\partial_{zz}\overline{u}_y - (C_{11}-C_{66})\partial_{xx}\overline{u}_x,\end{aligned} \tag{17}$$

where $\overline{\mathbf{u}} = (\overline{u}_x, \overline{u}_y)^\top$ represents the horizontal components of SH-wave in time-space domain, and $\overline{\mathbf{\Gamma}}_{\mathbf{m}}$ represents the Christoffel differential-operator matrix after the similarity transformation.

Due to the cylindrical symmetry of a TI material, the two equations in equation 17 may be summed to produce a scalar wave equation in terms of $\overline{u}$:

$$\rho\partial_{tt}\overline{u} = C_{66}(\partial_{xx}+\partial_{yy})\overline{u} + C_{44}\partial_{zz}\overline{u}, \tag{18}$$

with $\overline{u} = \overline{u}_x + \overline{u}_y$ representing the total horizontal components of the transformed SH-wave fields. This is consistent with the fact that only C_{44} and C_{66} affect the kinematic signatures of the SH-wave in VTI media (Tsvankin, 2001). In addition, the derived equation naturally reduces to the acoustic wave equation if we apply the isotropic assumption by setting $C_{44} = C_{66} = \rho {V_s}^2$ with V_s representing the velocity of the isotropic shear wave.

PSEUDO-PURE-MODE QSV-WAVE EQUATION

Derivation of pseudo-pure-mode qSV-wave equation

For the qSV-wave, we should essentially build a projection from the elastic wavefields $\widetilde{\mathbf{u}} = (\widetilde{u}_x, \widetilde{u}_y, \widetilde{u}_z)^\top$ to a pseudo-pure-mode wavefield $\widetilde{\overline{\mathbf{u}}} = (\widetilde{\overline{u}}_x, \widetilde{\overline{u}}_y, \widetilde{\overline{u}}_z)^\top$. Naturally, we may introduce the following similarity transformation to the Christoffel matrix, i.e.,

$$\widetilde{\overline{\mathbf{\Gamma}}}_{\mathbf{n}} = \mathbf{N}\widetilde{\mathbf{\Gamma}}\mathbf{N}^{-1}, \tag{19}$$

with the intuitive projection matrix $\mathbf{N}$ defined by the reference polarization direction $\mathbf{e}_3$:

$$\mathbf{N} = \begin{pmatrix} k_x k_z & 0 & 0 \\ 0 & k_y k_z & 0 \\ 0 & 0 & -(k_x^2 + k_y^2) \end{pmatrix}, \tag{20}$$

or its normalized form. However, the resulting pseudo-pure-mode wave equation is very complicated and contains mixed derivatives of time and space. To keep them simple, an intermediate wavefield $\widetilde{\overline{\mathbf{u}}}' = (\widetilde{u}_x, \widetilde{u}_y, \widetilde{u}'_z)^\top$ is defined by

$$\widetilde{\overline{u}}_z = (k_x^2 + k_y^2)\widetilde{\overline{u}}'_z. \tag{21}$$

So we project the vector displacement wavefields using:

$$\widetilde{\overline{\mathbf{u}}}' = \mathbf{N}'\widetilde{\mathbf{u}}, \tag{22}$$

with an intermediate projection matrix:

$$\mathbf{N}' = \begin{pmatrix} k_x k_z & 0 & 0 \\ 0 & k_y k_z & 0 \\ 0 & 0 & -1 \end{pmatrix}. \tag{23}$$

Accordingly, we apply the similarity transformation using $\mathbf{N}'$ to equation 3 and finally get an equivalent Christoffel equation:

$$\widetilde{\overline{\mathbf{\Gamma}}}'_{\mathbf{n}} \widetilde{\overline{\mathbf{u}}}' = \rho\omega^2 \widetilde{\overline{\mathbf{u}}}'. \tag{24}$$

with $\widetilde{\overline{\mathbf{\Gamma}}}'_{\mathbf{n}} = \mathbf{N}'\widetilde{\mathbf{\Gamma}}(\mathbf{N}')^{-1}$.

For a locally smooth medium, applying an inverse Fourier transformation to equation 24, we obtain another coupled forth-order linear system:

$$\rho\partial_{tt}\overline{\mathbf{u}}' = \overline{\mathbf{\Gamma}}'_{\mathbf{n}}\overline{\mathbf{u}}', \tag{25}$$

or in its extended form:

$$\begin{aligned}
\rho\partial_{tt}\overline{u}_x &= (C_{11}\partial_{xx} + C_{66}\partial_{yy} + C_{44}\partial_{zz})\overline{u}_x + (C_{11} - C_{66})\partial_{xx}\overline{u}_y + (C_{13} + C_{44})\partial_{xx}\partial_{zz}\overline{u}'_z, \\
\rho\partial_{tt}\overline{u}_y &= (C_{11} - C_{66})\partial_{yy}\overline{u}_x + (C_{66}\partial_{xx} + C_{11}\partial_{yy} + C_{44}\partial_{zz})\overline{u}_y + (C_{13} + C_{44})\partial_{yy}\partial_{zz}\overline{u}'_z, \\
\rho\partial_{tt}\overline{u}'_z &= (C_{13} + C_{44})\overline{u}_x + (C_{13} + C_{44})\overline{u}_y + C_{44}(\partial_{xx} + \partial_{yy})\overline{u}'_z + C_{33}\partial_{zz}\overline{u}'_z.
\end{aligned} \tag{26}$$

where $\overline{\mathbf{u}}' = (\overline{u}_x, \overline{u}_y, \overline{u}'_z)^\top$ is an intermediate wavefield in the time-space domain, and $\overline{\mathbf{\Gamma}}'_{\mathbf{n}}$ represents the corresponding Christoffel differential-operator matrix after the similarity transformation. The intermediate wavefield has the same horizontal components but a different vertical component of the pseudo-pure-mode wavefield $\overline{\mathbf{u}} = (u_x, u_y, u_z)^\top$. Equation 21 indicates that the vertical component satisfies:

$$\overline{u}_z = -(\partial_{xx} + \partial_{yy})\overline{u}'_z. \tag{27}$$

Due to the symmetry property of a VTI material, we may sum the horizontal components and replace the vertical component with the relation given in equation 27, and finally obtain a simpler second-order system that honors the kinematics of both qP- and qSV-waves:

$$\begin{aligned}\rho\partial_{tt}\overline{u}_{xy} &= C_{11}(\partial_{xx}+\partial_{yy})\overline{u}_{xy} + C_{44}\partial_{zz}\overline{u}_{xy} - (C_{13}+C_{44})\partial_{zz}\overline{u}_z,\\ \rho\partial_{tt}\overline{u}_z &= -(C_{13}+C_{44})(\partial_{xx}+\partial_{yy})\overline{u}_{xy} + C_{44}(\partial_{xx}+\partial_{yy})\overline{u}_z + C_{33}\partial_{zz}\overline{u}_z,\end{aligned} \tag{28}$$

with $\overline{u}_{xy} = \overline{u}_x + \overline{u}_y$. Note that pure SH-waves always polarize in the planes perpendicular to the symmetry axis with the polarization direction indicated by $\mathbf{e}_2$, which implies $(k_x k_z)\widetilde{u}_x + (k_y k_z)\widetilde{u}_y \equiv 0$, i.e., $\overline{u}_{xy} \equiv 0$, for the SH-wave. Therefore, the partial summation (after the similarity transformation) automatically removes the SH component from the transformed wavefields. As a result, there are no terms related to C_{66} any more in equation 28. In order to produce a pseudo-pure-mode scalar qSV-wave field, we sum all components of the transformed wavefields, namely

$$\overline{u} = \overline{u}_{xy} + \overline{u}_z. \tag{29}$$

For a 2-D VTI medium, equation 28 reduces to the following form:

$$\begin{aligned}\rho\partial_{tt}\overline{u}_x &= C_{11}\partial_{xx}\overline{u}_x + C_{44}\partial_{zz}\overline{u}_x - (C_{13}+C_{44})\partial_{zz}\overline{u}_z,\\ \rho\partial_{tt}\overline{u}_z &= -(C_{13}+C_{44})\partial_{xx}\overline{u}_x + C_{44}\partial_{xx}\overline{u}_z + C_{33}\partial_{zz}\overline{u}_z.\end{aligned} \tag{30}$$

In fact, we can derive the same pseudo-pure-mode wave equation for a 2-D qSV-wave by projecting the 2-D Christoffel matrix onto a reference vector $\mathbf{e}_3' = (k_z, -k_x)^\top$. Similarly, a 2D pseudo-pure-mode scalar qSV-wave field is given by the summation: $\overline{u} = \overline{u}_x + \overline{u}_z$.

If we apply the isotropic assumption by setting $C_{11} = C_{33}$ and $C_{13} + C_{44} = C_{33} - C_{44}$, and sum the two equations in equation 28, we get the scalar wave equation:

$$\rho\partial_{tt}\overline{u} = C_{44}(\partial_{xx}+\partial_{yy}+\partial_{zz})\overline{u}, \tag{31}$$

with $\overline{u} = \overline{u}_{xy} + \overline{u}_z$ representing a shear wave field, and $C_{44} = \rho {V_s}^2$ with V_s representing the propagation velocity of the isotropic shear wave.

The derived pseudo-pure-mode qSV-wave equations have some interesting and valuable features. First, the projection using matrix $\mathbf{N}$ yields wave-mode separation to some extent, because the chosen projection direction, $\mathbf{e}_3$, represents the polarization direction of the SV-wave in an isotropic medium. As investigated by Tsvankin and Chesnokov (1990) and Psencik and Gajewski (1998), and also demonstrated in Figure 1b, the difference in polarization directions between isotropic and VTI media is generally quite small in most propagation directions for SV-waves. Therefore, considering the mode separator (namely equation 9) and the small projection deviation, summing all the pseudo-pure-mode wavefield components in equation 28 or 30 partially achieves wave-mode separation and produces a scalar wavefield dominated by the energy of qSV-waves. This will be demonstrated in the numerical examples. Second, the pseudo-pure-mode wave equations are easier to calculate

than the original elastic wave equation because they have no terms of mixed partial derivatives. More importantly, the summation of the horizontal components further simplifies the wave equations and reduces the number of parameters needed for scalar qSV-wave extrapolation. These features are undoubtedly useful for performing multi-component seismic imaging and inversion that mainly use wavefield kinematics when it is necessary to include anisotropy.

Removing of the residual qP-waves

The pseudo-pure-mode qSV-wave equations are derived by using a similarity transformation that projects the vector displacement wavefield onto the isotropic reference of the qSV-wave's polarization direction. As demonstrated in Figure 1b, even for a very strong VTI medium, the difference bewteen the two directions is generally quite small in most propagation directions. However, this difference does result in some qP-wave energy remaining in the pseudo-pure-mode scalar qSV-wave fields. To remove the residual qP-waves, we have to correct the projection deviations before summing the pseudo-pure-mode wavefield components. For heterogeneous VTI media, this can be implemented through nonstationary spatial filtering defined by the projection deviations (Cheng and Kang, 2014).

The filters can be constructed once the qSV-wave polarization directions are determined by solving the Christoffel equation based on local medium properties for every grid point. However, this operation is computationally expensive, especially in 3D heterogeneous TI media. We may further reduce the computational cost using a mixed-domain integral algorithm using a low-rank approximation (Cheng and Fomel, 2014). We shall observe in the examples that the residual qP-waves in the pseudo-pure-mode qSV-wave fields are quite weak, even if the anisotropy becomes strong. As explained in Cheng and Kang (2014), it is not necessary to apply the filtering at every time step for many applications, such as RTM.

In the case of transverse isotropy with a tilted symmetry axis (TTI), the elastic tensor loses its simple form and the terminology "in-plane polarization" and "cross-plane polarization" is to be preferred for qSV- and qSH-waves. The generalization of pseudo-pure-mode wave equation to a TTI medium involves no additional physics but greatly complicates the algebra. One strategy for deriving the wave equations is to locally rotate the coordinate system so that its third axis coincides with the symmetry axis; and to make use of the simple form of the wave equation in VTI media (see Cheng and Kang (2014)). Alternatively, we may use some new strategies to derive more numerically stable pseudo-pure-mode wave equations for TTI media with strong variations of parameters (Zhang et al., 2011; Bube et al., 2012). Moreover, the filter to correct the projection deviation can also be constructed with the coordinate rotation.

EXAMPLES

The first example compares the synthetic elastic displacement and pseudo-pure-mode qSV-wave field in 2D homogeneous VTI media with different degrees of anisotropy. Then we demonstrate the computation of 3D synthetic pseudo-pure-mode qSV-wave and pure-mode SH-wave fields for a two-layer VTI model. Finally, we investigate the performance of the pseudo-pure-mode qSV-wave propagator on the 2D BP TTI model. We sue a tenth-order explicit finite-difference scheme on regular grids to solve the involved wave equations. Point sources are located at the centers of the models.

2D homogeneous VTI models

For comparison, we first apply the original elastic wave equation to synthesize wavefields in a homogeneous VTI medium with weak anisotropy, in which $v_{p0} = 3000m/s$, $v_{s0} = 1500m/s$, $\epsilon = 0.1$, and $\delta = 0.05$. Figures 2a and 2b display the horizontal and vertical components of the displacement wavefields at 0.3 s. Then we try to simulate the propagation of a single-mode qSV-wave using the pseudo-pure-mode qSV-wave equation (namely equation 30). Figure 2c and 2d display the two components of the pseudo-pure-mode qSV-wave fields, and Figure 2e displays their summation, i.e., the pseudo-pure-mode scalar qSV-wave fields with weak residual qP-wave energy. We observe that, in most propagation directions, the polarities are almost reversed for the wavefronts of qP-waves in the two components of the pseudo-pure-mode qSV-wave fields. This contributes to suppressing the qP-wave energy through summation of the two components. Compared with the theoretical wavefront curves (see Figure 2f) calculated using group velocities and angles, pseudo-pure-mode scalar qSV-wave fields have correct kinematics for both qP- and qSV-waves. We finally remove residual qP-waves by applying the filtering to correct the projection deviation and get completely separated scalar qSV-wave fields (Figure 2g).

Next, we consider wavefield modeling in a homogeneous VTI medium with strong anisotropy, in which $v_{p0} = 3000m/s$, $v_{s0} = 1500m/s$, $\epsilon = 0.25$, and $\delta = -0.25$. Figure 3 displays the wavefield snapshots at 0.3 s synthesized both by using the original elastic wave equation and the pseudo-pure-mode qSV-wave equation. Note that the pseudo-pure-mode qSV-wave equation still accurately represents the qP- and qSV-waves' kinematics. Although the residual qP-wave energy becomes stronger when the degree of anisotropy increases, the filtering step still removes them effectively. It takes CPU times of 0.15 and 0.06 seconds to extrapolate the elastic and pseudo-pure-mode qSV-wave fields for one time-step, respectively. But it takes about 8.2 seconds to remove the residual qP-wave from the pseudo-pure-mode qSV-wave fields using wavenumber-domain filtering. In fact, separating the pure-mode wavefield from the elastic and pseudo-pure-mode wavefields has almost the same computational cost for TI media (Cheng and Kang, 2014).

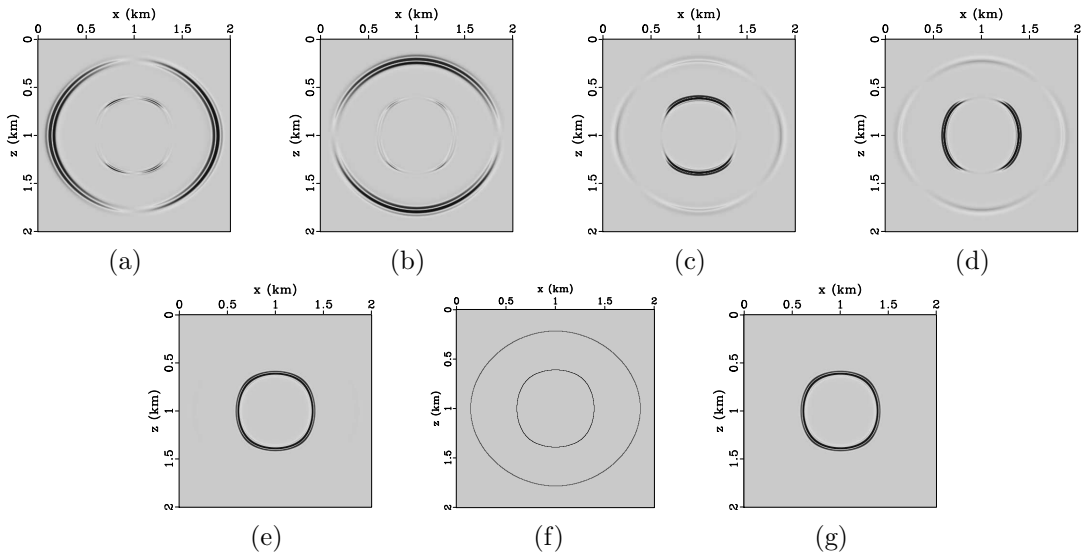

Figure 2: Synthesized wavefields in a VTI medium with weak anisotropy: (a) x- and (b) z-components synthesized by original elastic wave equation; (c) x- and (d) z-components synthesized by pseudo-pure-mode qSV-wave equation; (e) pseudo-pure-mode scalar qSV-wave fields; (f) kinematics of qV- and qSV-waves and (g) separated scalar qSV-wave fields.

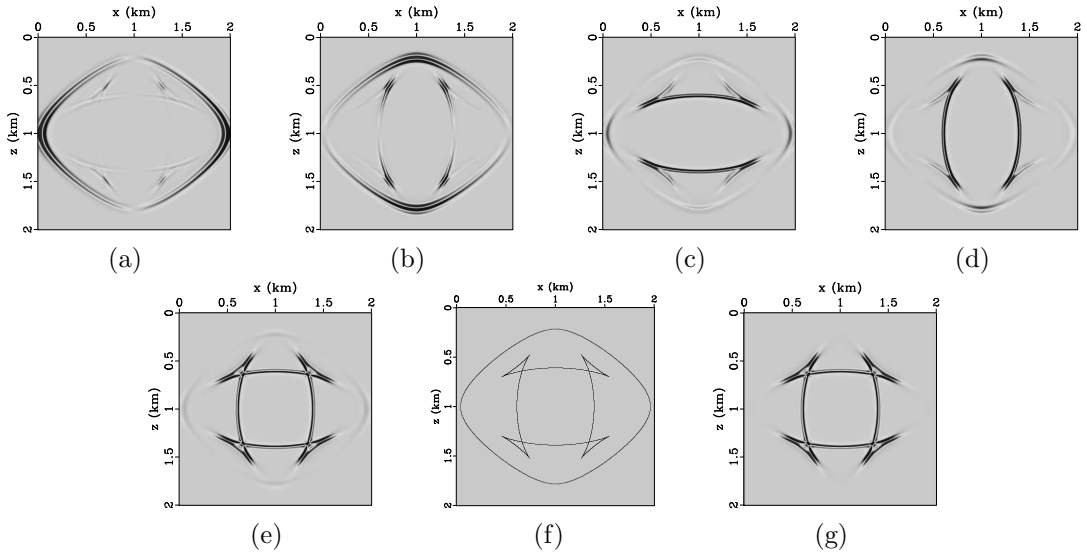

Figure 3: The same plots as Figure 2 but for a VTI medium with stronger anisotropy.

3D two-layer VTI model

Figure 4 shows an example of simulating the propagation of pseudo-pure-mode qSV-wave fields in a 3D two-layer VTI model (see Figure 4a), with $v_{p0} = 2500m/s$, $v_{s0} = 1200m/s$, $\epsilon = 0.25$, $\delta = -0.25$ and $\gamma = 0.3$ in the first layer, and $v_{p0} = 3600m/s$, $v_{s0} = 1800m/s$, $\epsilon = 0.2$, $\delta = 0.1$ and $\gamma = 0.05$ in the second layer. We propagate the 3D pseudo-pure-mode qSV-wave fields using equation 28. Figure 4d displays the pseudo-pure-mode scalar qSV-wave fields resulting from the summation of the horizontal (Figure 4b) and vertical (Figure 4c) components, namely $\overline{u}_{xy}$ and $\overline{u}_z$. We see that the qS-waves dominate the scalar wavefields in energy. As shown in Figure 5, we also obtain pure-mode scalar SH-wave fields either using the summation of the horizontal components synthesized by using the pseudo-pure-mode wave equation 17 or directly using the scalar wave equation, i.e., equation 18.

BP 2007 TTI model

Finally, we demonstrate pseudo-pure-mode qSV-wave propagation in the 2D BP TTI model (see Figure 6). The space grid size is 12.5 m and the time step is 1 ms for high-order finite-difference operators. Here the vertical velocities for the qSV-wave are set to half of the qP-wave velocities. Figure 7 displays snapshots of wavefield components at the time of 1.4s synthesized by using the original elastic wave equation and the pseudo-pure-mode qSV-wave equation. In the elastic wavefields, we observe strong scattered and mode-converted energy in the region with a rapidly varying anisotropic symmetry axis direction. For comparison, in Figures 7c and 7d, we also show the separated qP- and qSV-wave scalar fields obtained using the approach proposed by Cheng and Fomel (2014). Not that in the pseudo-pure-mode qSV-wave fields (see Figure 7g), the incident qP-waves as well as scattered and converted qP-waves are effectively suppressed. The spatial filtering appears to remove residual qP-waves and accurately separates qSV-wave data (including the converted qP-qSV waves) from the pseudo-pure-mode wavefields in this complex model (Figure 7h). Vertical slices through the scalar fields (Figure 8) provide further proof to evaluate the performance of the proposed qS-wave propagators. As we observed, in heterogeneous rough zones with strong variations in tilt angle, there are differences between the elastic and pseudo-pure-mode qSV-wave fields. Fortunately, the pseudo-pure-mode qSV-wave equation still captures the shear wave kinematics to a great extent. For a single time-step, it respectively takes CPU times of 2.71 and 1.22 seconds to extrapolate the elastic and pseudo-pure-mode qSV-wave fields, and about 7.50 seconds to separate the qSV-wave fields from both wavefields using low-rank approximate mixed-domain integral operations based on the qSV-wave's polarization directions (Cheng and Fomel, 2014).

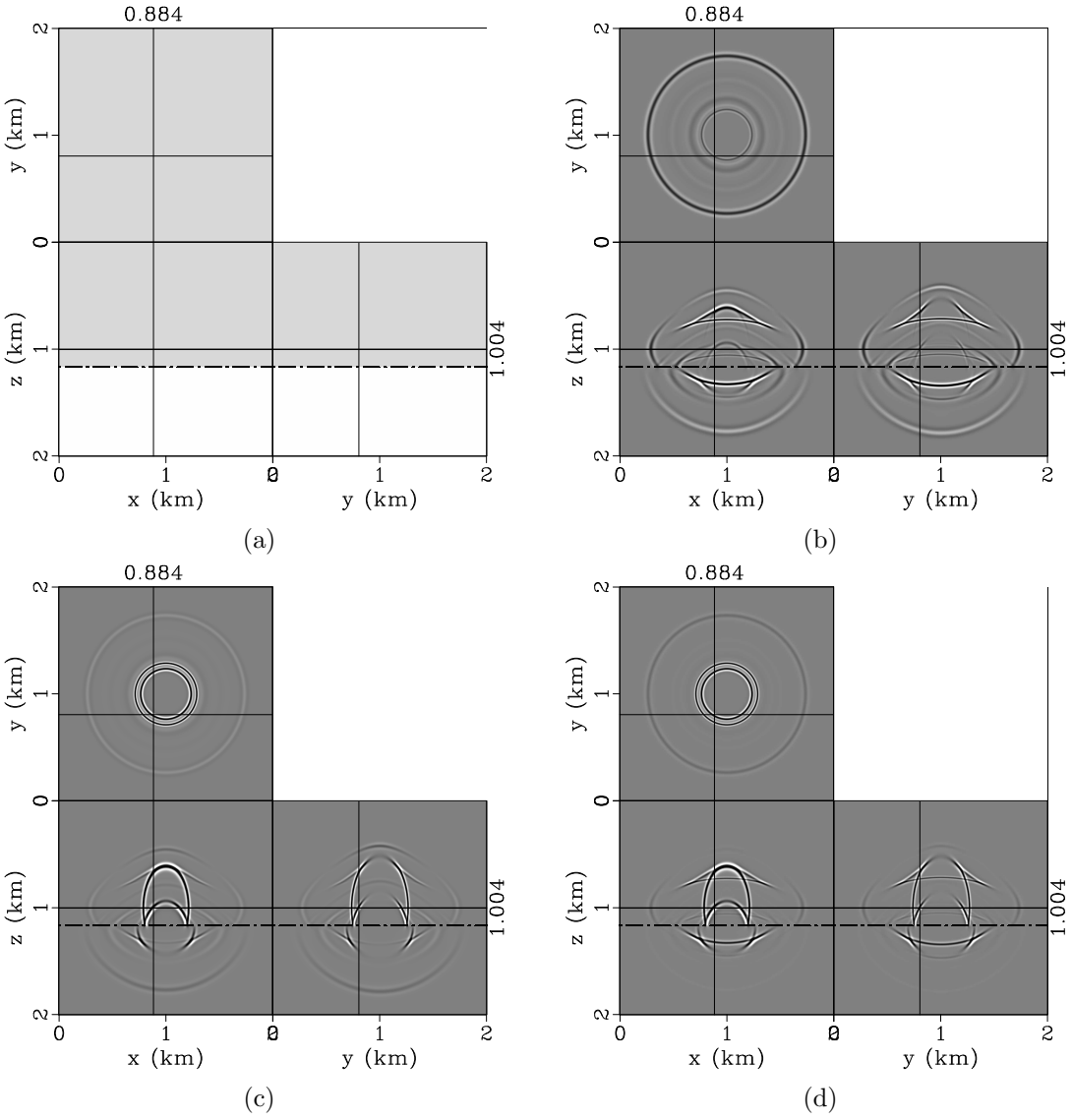

Figure 4: Synthesized wavefield snapshots in a 3D two-layer VTI model using equation 28 : (a) vertical velocity of qSV-wave, (b) horizontal component $\overline{u}_{xy}$ and (c) vertical component $\overline{u}_z$ of the pseudo-pure-mode qSV-wave fields, (d) pseudo-pure-mode scalar qSV-wave fields. The dash line indicates the interface.

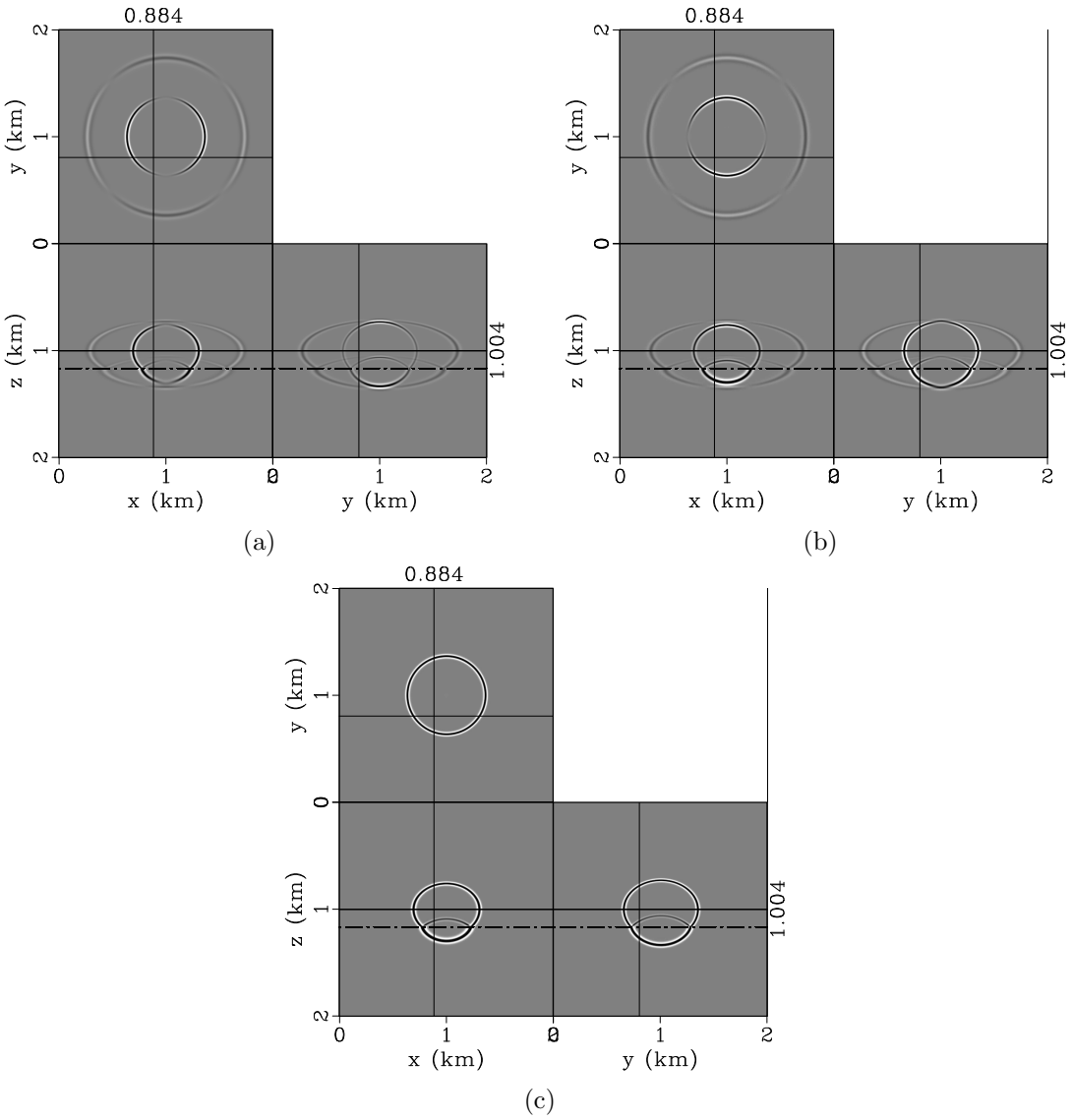

Figure 5: Synthesized wavefield snapshots in a 3D two-layer VTI model using equation 17: (a) x- and (b) y-components of the pseudo-pure-mode wavefields, (c) pure-mode scalar SH-wave fields calculated as the summation of the two horizontal components of the pseudo-pure-mode wavefields. Note that the same scalar wavefields are obtained if we directly use the scalar wave equation for SH-waves, namely equation 18.

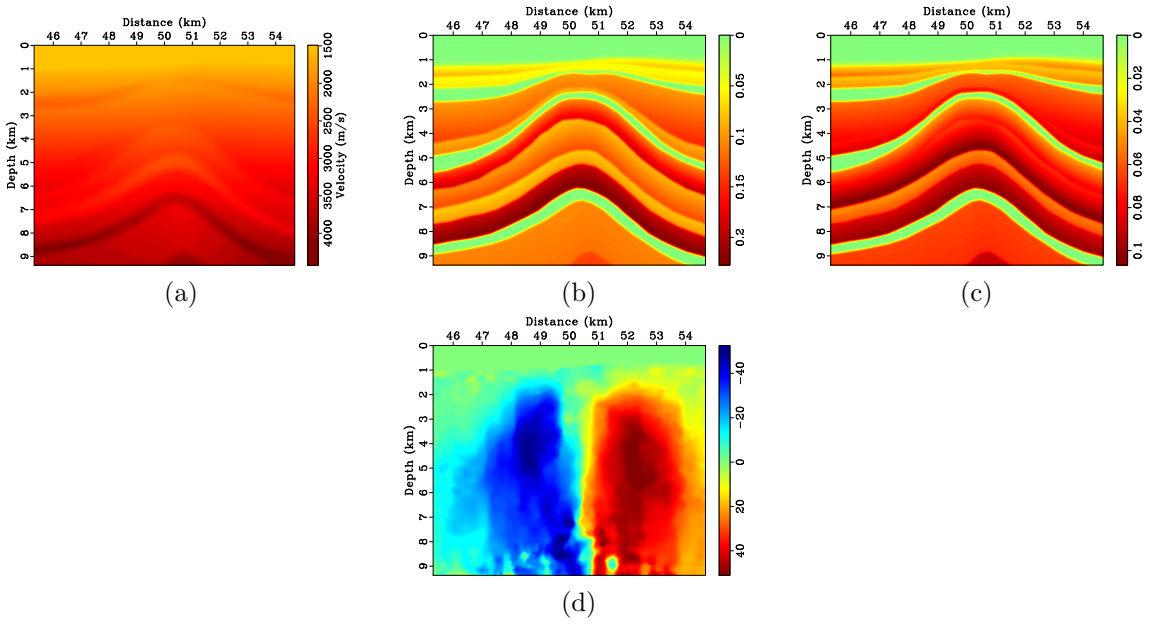

Figure 6: Partial region of the 2D BP TTI model: (a) vertical qP-wave velocity, Thomsen coefficients (b) ϵ and (c) δ, and (d) the tilt angle θ.

DISCUSSION

Kinematic and dynamic accuracy

The similarity transformation to the Christoffel equation preserves the kinematics of the qS-waves, but inevitably change the phases and amplitudes in their wavefields. Accordingly, the pseudo-pure-mode wave equations may change the radiation from a point source (as demonstrated in the examples), and even distort the amplitude variation with offset (AVO). In other word, they do not honor the dynamic elasticity of the waves in real media. In fact, other simplified forms of the elastic wave equation, such as acoustic or pseudo-acoustic wave equations and the pure-mode approximate wave equations, have similar limitations (Barnes and Charara, 2009; Operto et al., 2009; Cheng and Kang, 2014; Shang et al., 2015). For heterogeneous rough media, i.e., when scales for variations in the elastic parameters are small compared with the wavelengths of the wavefield, the acoustic approximation is no longer reliable (Cance and Capdeville, 2015). The pseudo-pure-mode wave equations have similar limitations for shear-wave modeling in high-contrast TI media. However, these limitations are not doomed to be catastrophic, because velocity models containing high-wavenumber components are rarely involved at most stages of seismic imaging and inversion for real data.

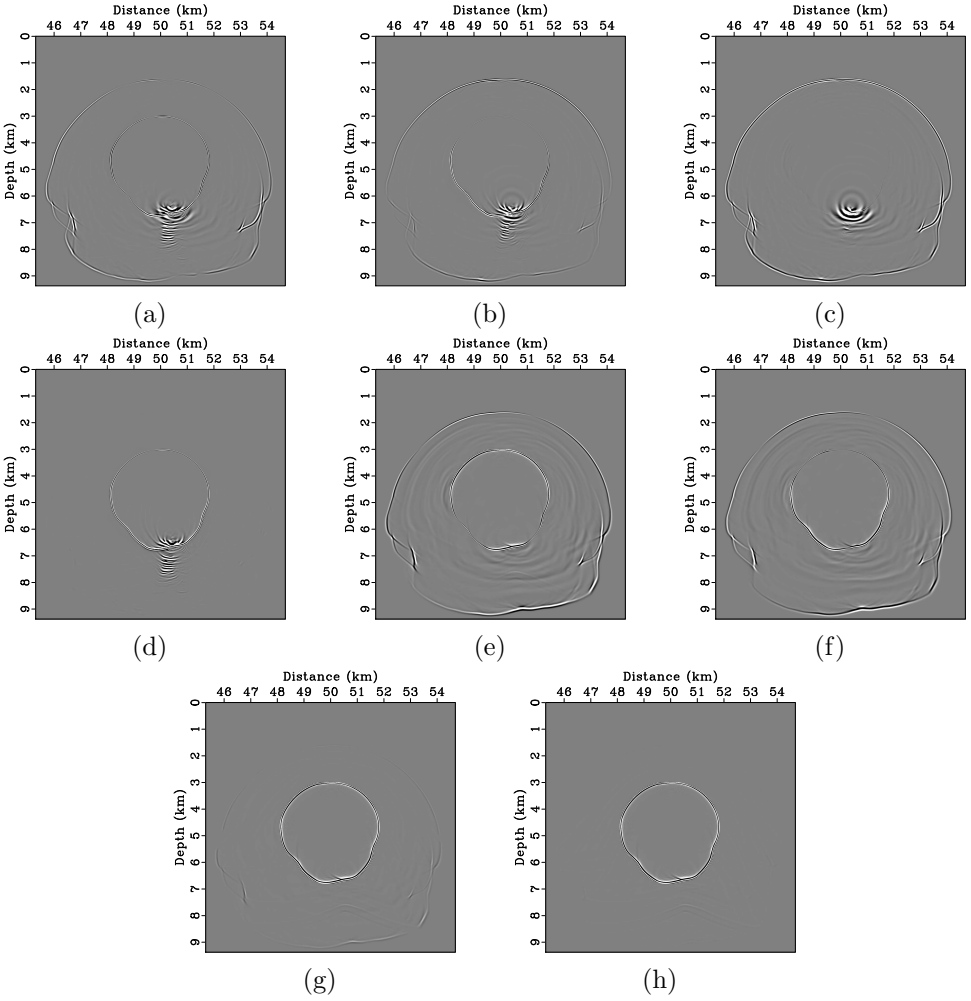

Figure 7: Synthesized wavefield snapshots on BP 2007 TTI model using original elastic wave equation and pseudo-pure-mode qSV-wave equation respectively: (a) x- and (b) z-components synthesized by elastic wave equation; (c) scalar qP- and (d) scalar qSV-wave fields separated from the elastic wavefield; (e) x- and (f) z-components synthesized by pseudo-pure-mode qSV-wave equation; (g) pseudo-pure-mode scalar qSV-wave field and (h) pure-mode scalar qSV-wave field separated from the pseudo-pure-mode qSV-wave field.

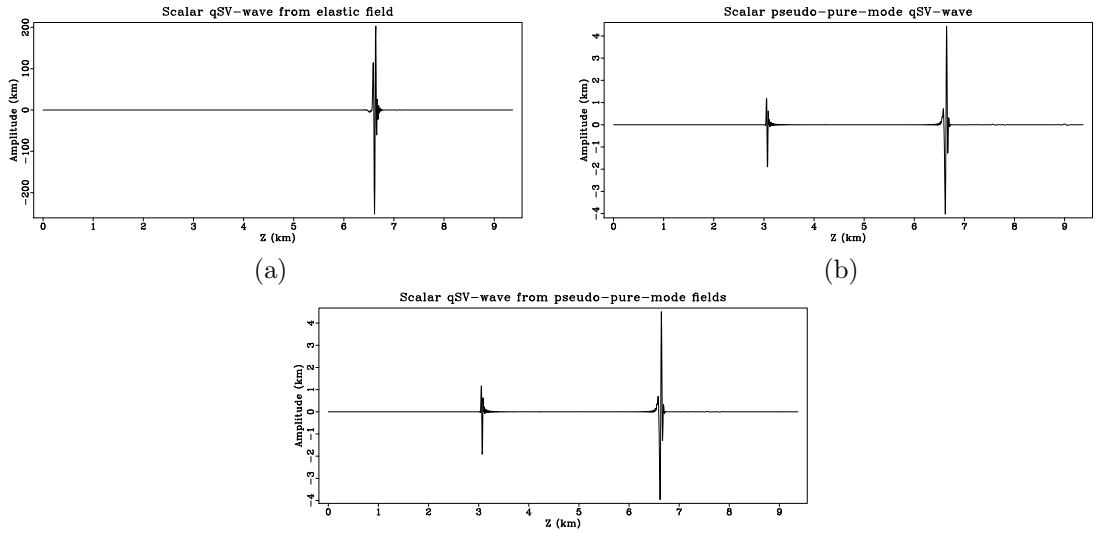

Figure 8: Vertical slices through the scalar wavefields at $x = 50.5$ km in Figure 7: (a) qSV-wave separated from the elastic wavefield; (b) pseudo-pure-mode qSV-wave; (c) pure qSV-wave separated from the pseudo-pure-mode wavefield.

Challenge for anisotropy with lower symmetry

Unlike the well-behaved qP-wave mode, the qS-wave modes do not consistently polarize as a function of propagation direction, and thus cannot be designated as SV- and SH-waves, except in isotropic and TI media (Winterstein, 1990). To demonstrate the difficulties of extending the methodology in this paper to anisotropic media with symmetry lower than TI, we first compare the polarization features of qS-waves in typical TI and orthorhombic anisotropic rocks. Figure 9 shows polarizations of qS1- and qS2-waves in a VTI material - Mesaverde shale (Thomsen, 1986), which has the parameters $v_{p0} = 3.749$ km/s, $v_{s0} = 2.621$ km/s, $\epsilon = 0.225$, $\delta = 0.078$, and $\gamma = 0.100$. The polarization directions are either horizontal or vertical (in the symmetry plane), so that we can definitely designate qS-waves as qSV- and SH-wave modes, except at the kiss singularity. Figure 10 shows polarizations of qS1- and qS2-waves in a "standard" orthorhombic anisotropic material - vertically fractured shale (Schoenberg and Helbig, 1997), which has the parameters $v_{p0} = 2.437$, $v_{s0} = 1.265$ km/s, $\epsilon_1 = 0.329$, $\epsilon_2 = 0.258$, $\delta_1 = 0.083$, $\delta_2 = -0.078$, $\delta_3 = -0.106$, $\gamma_1 = 0.182$ and $\gamma_2 = 0.0455$. The qS-waves polarize in a very complicated way and have point singularities in many propagation directions.

Shear-wave modeling is complicated by the presence of the shear-wave singularities. As investigated by Crampin and Yedlin (1981), a TI material only has line and kiss singularities, while other anisotropic materials excluding those with triclinic symmetry (e.g., orthorhombic and monoclinic anisotropic materials) have point singularities in many propagation directions. Line singularities occur only at a fixed

angle from the symmetry axis and cause no distortion of phase velocity surfaces or polarization phenomena. For kiss singularities (along the direction of symmetry axis), qS-wave polarizations vary rapidly in their vicinity but are well-behaved because there is no distortion in phase-velocity surfaces. These features facilitate the derivations of pseudo-pure-mode qSV-wave and pure-mode SH-wave equations for TI media. For directions near point singularities, however, the polarization of plane qS-waves changes very rapidly, and amplitudes and polarizations of qS-waves with curved wavefronts behave quite anomalously. Therefore, although pseudo-pure-mode qP-wave equations exist for general anisotropic media, it may be more confusing than helpful to extend the proposed pseudo-pure-mode qS-wave equations to symmetry systems lower than TI.

CONCLUSIONS

By applying two different similarity transformations to the original Christoffel equation, which aim to project the vector displacement wavefields onto the isotropic SV- and SH-waves' polarization directions, we have derived the pseudo-pure-mode qSV-wave equation and the pure-mode SH-wave equation for 2D and 3D heterogeneous TI media, respectively. These equations are simpler than the original elastic wave equation and involve less material parameters, which reduces computational cost at least by half if the finite-difference scheme is used in practice. The theoretical analysis and numerical examples have demonstrated that, the pseudo-pure-mode qS-wave propagators for TI media have the following features: First, the qSV-wave equations honor the kinematics for both qP and qSV modes, while the pure-mode SH-wave equation guarantees the kinematics for the scalar SH-wave. Second, although qP-waves still remain in the pseudo-pure-mode qSV-wave fields, their horizontal and vertical components have almost opposite polarities in most propagation directions. As a result, the summation of all components produces a pseudo-pure-mode scalar qSV-wave field with very weak qP-wave energy. Third, the non-SH parts in the pseudo-pure-mode vector SH-wave field have completely opposite polarities, and thus are thoroughly removed from the scalar SH-wave field once all components are summed. In addition, a filtering step taking into account the polarization deviation can be used to thoroughly remove the residual qP-waves for pseudo-pure-mode scalar qSV-wave extrapolation. These features indicate the potential of the proposed qS-wave propagators for developing promising seismic imaging and inversion algorithms in heterogeneous TI media. Like the pseudo-acoustic or pseudo-pure-mode qP-wave equations, the proposed pseudo-pure-mode qS-wave equations take into account "scalar anisotropy" and may distort the dynamic elasticity of the real anisotropic media.

ACKNOWLEDGMENTS

Thanks to the support of the National Natural Science Foundation of China (No.41474099) and Shanghai Natural Science Foundation (No.14ZR1442900). We appreciate Sergey

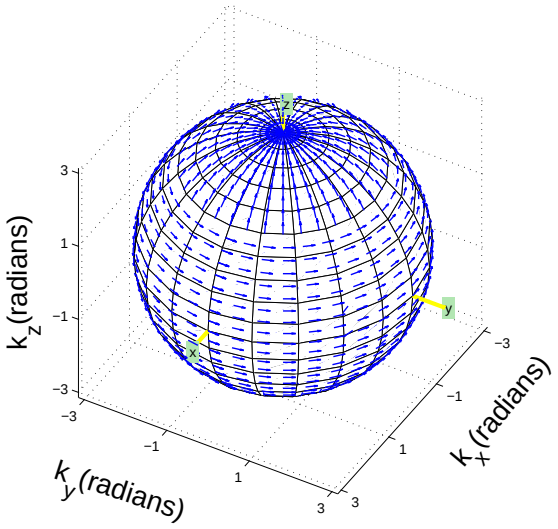

(a)

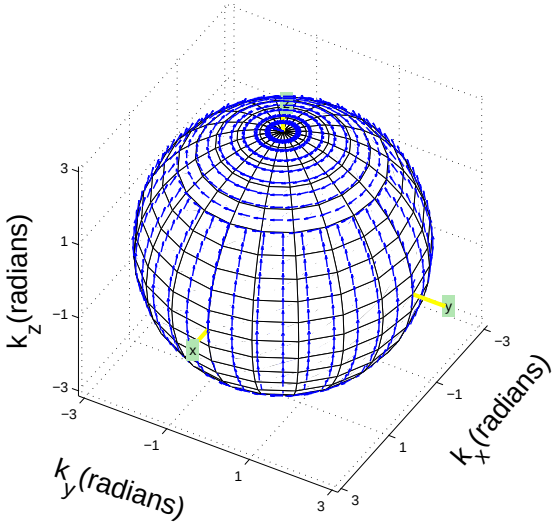

(b)

Figure 9: Polarization vectors of 3D qS-waves in a VTI material (Mesaverde shale): (a) qS1-wave; (b) qS2-wave.

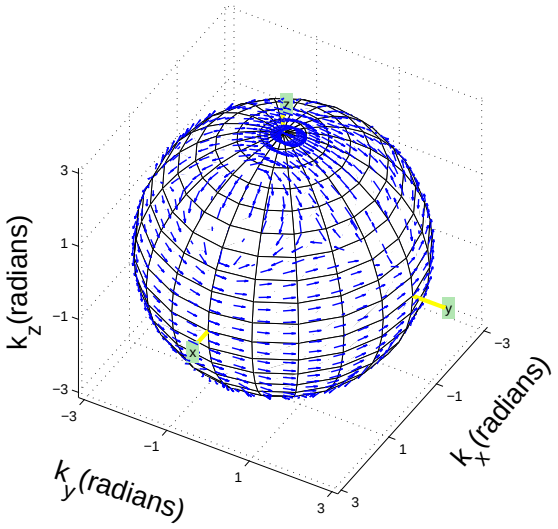

(a)

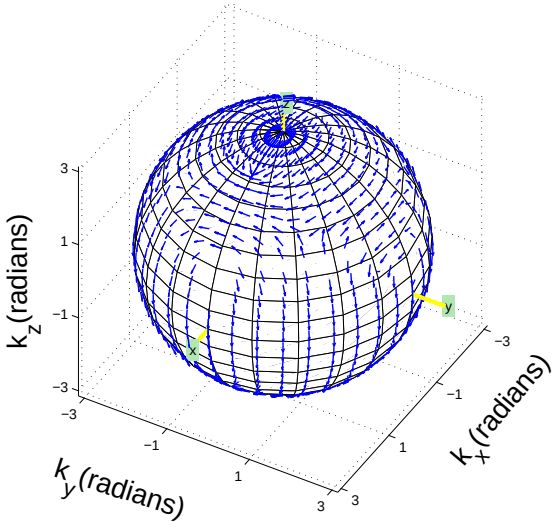

(b)

Figure 10: Polarization vectors of 3D qS-waves in an orthorhombic anisotropic material: (a) qS1-wave; (b) qS2-wave.

Fomel, Paul Fowler, Chenlong Wang and Tengfei Wang for helpful discussions in the later period of this study. Constructive comments by Richard Bale, Alexey Stovas, Joe Dellinger and an anonymous reviewer are much appreciated. We thank SEG and BP for making the 2D TTI model available, and the authors and developers of *Madagascar* for providing resources for reproducible computational experiments.

REFERENCES

Alkhalifah, T., 2000, An acoustic wave equation for anisotropic media: Geophysics, **65**, 1239–1250.

———, 2003, An acoustic wave equation for orthorhombic anisotropy: Geophysics, **68**, 1169–1172.

Baig, A., and T. Urbancic, 2010, Microseismic moment tensors: A path to understanding frac growth: The Leading Edge, **29**, 320–324.

Barnes, C., and M. Charara, 2009, The domain of applicability of acoustic full-waveform inversion for marine seismic data: Geophysics, **74**, WCC91–WCC103.

Bube, K. P., T. Nemeth, J. P. Stefani, R. Ergas, W. Liu, K. T. Nihei, and L. Zhang, 2012, On the instability in second-order systems for acoustic VTI and TTI media: Geophysics, **77**, T171–T186.

Cance, P., and Y. Capdeville, 2015, Validity of the acoustic approximation for elastic waves in heterogeneous media: Geophysics, **80**, T161–T173.

Carcione, J. M., 2007, Wave fields in real media: Wave propagation in anisotropic, anelastic, porous and electromagnetic media: Pergamon Press.

Cary, P. W., 2001, Multicomponent seismic exploration in Canada - One person's perspective: Recorder, **26**, 62–67.

Cerveny, V., and J. Jech, 1982, Linearized solutions of kinematic problems of seismic body waves in inhomogeneous slightly anisotropic media: Journal of Geophysics, **51**, 96–104.

Cheng, J. B., and S. Fomel, 2014, Fast algorithms of elastic wave mode separation and vector decomposition using low-rank approximation for anisotropic media: Geophysics, **79**, C97–C110.

Cheng, J. B., and W. Kang, 2014, Simulating propagation of separated wave modes in general anisotropic media, Part I: qP-wave propagators: Geophysics, **79**, C1–C18.

Chu, C., B. Macy, and P. Anno, 2011, Approximation of pure acoustic seismic wave propagation in TTI media: Geophysics, **76**, WB98–WB107.

Crampin, S., 1991, Effective of point singularities on shear-wave propagation in sedimentary basins: Geophysical Journal International, **107**, 531–543.

Crampin, S., and M. Yedlin, 1981, Shear-wave singularities of wave propagation in anisotropic media: Journal of Geophysics, **49**, 43–46.

Crawley, S., S. Brandsberg-Dahl, and J. McClean, 2010, 3D TTI RTM using the pseudo-analytic method: 80th Annual International Meeting, SEG, Expanded Abstracts, 3216–3220.

Dellinger, J., 1991, Anisotropic seismic wave propagation: PhD thesis, Stanford University.

Dellinger, J., and J. Etgen, 1990, Wavefield separation in two-dimensional anisotropic media: Geophysics, **55**, 914–919.

Djebbi, R., and T. Alkhalifah, 2014, Analysis of the multi-component pseudo-pure-mode qP-wave inversion in vertical transverse isotropic (VTI) media: 84nd Annual International Meeting, SEG, Expanded Abstracts, 394–399.

Du, X., P. J. Fowler, and R. P. Fletcher, 2014, Recursive integral time-extrapolation methods for waves: A comparative review: Geophysics, **79**, T9–T26.

Duveneck, E., and P. M. Bakker, 2011, Stable P-wave modeling for reverse-time migration in tilted TI media: Geophysics, **76**, S65–S75.

Etgen, J., and S. Brandsberg-Dahl, 2009, The pseudo-analytical method: Application of pseudo-Laplacians to acoustic and acoustic anisotropic wave propagation: 79th Annual International Meeting, SEG, Expanded Abstracts, 2552–2556.

Farra, V., 2001, High-order perturbations of the phase velocity and polarization of qp and qs waves in anisotropic media: Geophysical Journal International, **147**, 93–104.

Fletcher, R. P., X. Du, and P. J. Fowler, 2009, Reverse time migration in tilted transversely isotropic (TTI) media: Geophysics, **74**, WCA179–WCA187.

Fomel, S., L. Ying, and X. Song, 2013, Seismic wave extrapolation using lowrank symbol approximation: Geophysical Prospecting, **61**, 526–536.

Fowler, P. J., X. Du, and R. P. Fletcher, 2010, Recursive integral time extrapolation methods for scalar waves: 80th Annual International Meeting, SEG, Expanded Abstracts, 3210–3215.

Fowler, P. J., and R. King, 2011, Modeling and reverse time migration of orthorhombic pseudo-acoustic P-waves: 81st Annual International Meeting, SEG, Expanded Abstracts, 190–195.

Grechka, V., and S. Yaskevich, 2014, Azimuthal anisotropy in microseismic montoring: A Bakken case study: Geophysics, **79**, KS1–KS12.

Grechka, V., L. Zhang, and J. W. Rector, 2004, Shear waves in acoustic anisotropic media: Geophysics, **69**, 576–582.

Hardage, B. A., M. V. DeAngelo, P. E. Murray, and D. Sava, 2011, Multicomponent seismic technology: SEG.

Helbig, K., 1994, Foundation of anisotropy for exploration seismics: Pergamon Press.

Li, X. Y., 1997, Fractured reservoir delineation using multicomponent seismic data: Geophysical Prospecting, **45**, 39–64.

Liu, F., S. Morton, S. Jiang, L. Ni, and J. Leveille, 2009, Decoupled wave equations for P and SV waves in an acoustic VTI media: 79th Annual International Meeting, SEG, Expanded Abstracts, 2844–2848.

Maxwell, S., 2010, Microseismic: Growth born from success: The Leading Edge, 338–343.

Musgrave, M. J. P., 1970, Crystal acoustics: Holden Day.

Operto, S., J. Virieux, A. Ribodetti, and J. E. Anderson, 2009, Finite-difference frequency-domain modeling of viscoacoustic wave propagation in 2D tilted transversely isotropic (TTI) media: Geophysics, **74**, T75–T95.

Pestana, R., B. Ursin, and P. L. Stoffa, 2011, Separate P- and SV-wave equations for VTI media: SEG Technical Program Expanded Abstracts, 163–167.

Psencik, I., and D. Gajewski, 1998, Polarization, phase velocity, and NMO velocity of qP-waves in arbitrary weak anisotropic media: Geophysics, **63**, 1754–1766.

Schoenberg, M., and K. Helbig, 1997, Orthorhombic media: Modeling elastic wave behavior in a vertically fractured earth: Geophysics, **62**, 1954–1974.

Shang, Y. X., J. B. Cheng, and T. F. Wang, 2015, Investigation of amplitude accuracy for pseodu-acoustic wave propagation in azimuthal anisotropic media: EAGE Technical Program Expanded Abstracts, accepted.

Song, X., S. Fomel, and L. Ying, 2013, Lowrank finite-difference and lowrank Fourier finite-differences for seismic wave extrapolation in the acoustic approximation: Geophysical Journal International, **193**, 960–969.

Stewart, R., J. Gaiser, R. Brown, and D. Lawton, 2002, Converted-wave seismic exploration: Method: Geophysics, **67**, 1348–1363.

Thomsen, L., 1986, Weak elastic anisotropy: Geophysics, **51**, 1954–1996.

———, 1999, C-wave reflection seismology over inhomogeneous and anisotropic media: Geophysics, **64**, 678–690.

Tsvankin, I., 2001, Seismic signatures and analysis of reflection data in anisotropic media: Elsevier Science Ltd.

Tsvankin, I., and E. Chesnokov, 1990, Synthesis of body-wave seismograms from point source in anisotropic media: Journal of Geophysics Research, **95**, 11317–11331.

Winterstein, D. F., 1990, Velocity anisotropy terminology for geophysicists: Geophysics, **55**, 1070–1088.

Xu, S., and H. Zhou, 2014, Accurate simulations of pure quasi-P-waves in complex anisotropic media: Geophysics, **79**, T341–T348.

Yan, J., and P. Sava, 2011, Improving the efficiency of elastic wave-mode separation for heterogenous tilted transver isotropic media: Geophysics, **76**, T65–T78.

Yu, V., V. Grechka, and I. R. Obolentseva, 1993, Geometrical structure of shear wave surface near singularity directions in anisotropic media: Geophysical Journal Internation, **115**, 609–616.

Zhan, G., R. C. Pestana, and P. L. Stoffa, 2012, Decoupled equations for reverse time migration in tilted transversely isotropic media: Geophysics, **77**, T37–T45.

Zhang, H., G. Zhang, and Y. Zhang, 2009, Removing S-wave noise in TTI reverse time migration: 79th Annual International Meeting, SEG, Expanded Abstracts, 2849–2853.

Zhang, H., and Y. Zhang, 2011, Reverse time migration in vertical and tilted orthorhombic media: 81st Annual International Meeting, SEG, Expanded Abstracts, 185–189.

Zhang, L., J. W. Rector, and G. M. Hoversten, 2005, Finite-difference modeling of wave propagation in acoustic TI media: Geophysical Prospecting, **53**, 843–852.

Zhang, Q., and G. A. McMechan, 2010, 2D and 3D elastic wavefield vector decomposition in the wavenumber domain for VTI media: Geophysics, **75**, D13–D26.

Zhang, Y., and G. Zhang, 2009, One-step extrapolation method for reverse time migration: Geophysics, **74**, A29–A33.

Zhang, Y., H. Zhang, and G. Zhang, 2011, A stable TTI reverse time migration and its implementation: Geophysics, **76**, WA3–WA11.

Zhou, H., G. Zhang, and R. Bloor, 2006, An anisotropic acoustic wave equation

for VTI media: 68th Annual International Meeting, EAGE, Expanded Abstracts, 1171–1174.